

# Optimal Design of a Dual Active Bridge DC-DC Converter

Dibakar Das, *Student Member, IEEE* and Kaushik Basu, *Member, IEEE*

**Abstract**—This paper presents a systematic design procedure for a Dual active bridge (DAB) DC-DC converter. Design of a DAB converter involves determination of two key parameters i.e. transformer turns ratio and the series inductance value. Existing literature addresses this problem through numerical optimization which is computation intensive and does not provide much insight. In general loss is minimized by applying equal weightage to all operating conditions, which may not be practical. Given an operating power range, terminal voltage range and switching frequency, this paper presents a way to optimally select the design variables through analytical solution of a constrained optimization problem. Analysis is carried out in time domain and optimal triple phase shift modulation strategy is considered that ensures minimum inductor rms current and soft switching. The choice of the design parameters results in minimization of the worst-case inductor rms current over the entire operating range of the converter which leads to both efficiency and size optimization. A procedure for selection of devices and filter capacitors and design of magnetics is given. A 2.6kW experimental prototype is designed to validate the theoretical analysis.

**Index Terms**—Dual active bridge, RMS current minimization, TPS modulation, Soft switching, Optimal design

## NOMENCLATURE

$V_1$	Voltage of the controlled port.
$V_2$	Voltage of the uncontrolled port.
$i_L$	Instantaneous inductor current.
$I_{rms}$	Actual value of inductor rms current.
$i_{rms}$	Scaled value of inductor rms current.
$P$	Average power transferred between the DC ports.
$p$	Scaled value of average transferred power.
$f_s$	Switching frequency of the converter.
$n$	Turns ratio of the transformer.
$L$	Total series inductance of the DAB converter.
$d_1$	Duty cycle of primary voltage waveform.
$d_2$	Duty cycle of secondary voltage waveform.
$\delta$	Phase shift between primary and secondary voltage waveforms.
$m$	Voltage conversion ratio.

## I. INTRODUCTION

**D**UAL Active Bridge (DAB) converters are a desirable choice in DC-DC power conversion since they have several beneficial features such as galvanic isolation, bidirectional

power flow capability, soft switching leading to high efficiency and power density [1]. These converters are used in several applications such as DC microgrids, battery chargers, solid state transformers, etc.

In dual active bridge topology, two H-bridge converters apply square waveforms to transformer primary and secondary windings in series with an inductor. A phase shift is introduced between the waveforms for power transfer, [2]. This modulation strategy is known as single phase shift strategy (SPS) in literature. Later, it was found that introducing duty modulation in primary and secondary voltages can lead to several advantages, [3]. This three degree of freedom in modulation (two duty cycles and phase shift) is known as triple phase shift (TPS) strategy in literature, [3]. The TPS strategy is considered in this paper.

Several methods exist in literature which address the optimal modulation problem based on minimization of a given objective function. In such problems, for a specified operating condition (power, voltage, switching frequency) and a given design (transformer turns ratio, series inductance value), the objective is to determine the TPS modulation parameters which will minimize power loss. For loss minimization, one popular approach is using fundamental approximation [4]–[7] of the voltage and current waveform and minimize the circulating [4], [5] or reactive component [6], [7] of the inductor current. Although this approach leads to a simpler analysis, the approximations may not be valid over a wide operating range of the converter. A more general method that results in accurate prediction over a wide range of operation is to use time-domain expressions for power and inductor current [3], [8]–[10].

Considering time domain analysis, the objective function for minimization may be inductor rms current [8]–[10], peak current [11]–[15], soft switching [3], [16] or total loss [17]–[19]. Out of the above alternatives for the objective function, the rms of the inductor current with soft switching is a suitable candidate for optimization because it represents the conduction losses in the devices and the magnetic components which form a major fraction of the total loss of the converter, [8]. Moreover, reducing the rms of inductor current also implies reduction of peak currents and capacitor ripple current ratings.

Several approaches for minimization of rms currents through time domain exact analysis can be found in literature. A numerical approach for choosing optimal TPS parameters can be found in [8]. The proposed strategy has three regions of operation based on the power output of the converter. A more formal treatment of the rms current minimization problem and an analytical solution can be found in [10]. Though soft switching is not included in the problem formulation, it is shown that the results satisfy the soft switching constraints.

In a typical DC-DC converter, the voltage at one port is

Manuscript received May 29, 2020; revised November 10, 2020; accepted November 26, 2020. The authors are with the Department of Electrical engineering, Indian Institute of Science, Bangalore, 560012, India (e-mail: dibakard@iisc.ac.in, kbasu@iisc.ac.in). This work was supported by the Indian Space Research Organisation, Government of India under the project titled “Development of AC power system for satellite applications”.

tightly regulated despite variations in the other port voltage. The design specifications include voltage at the regulated port, the range of unregulated port voltage, range of operating power and the switching frequency, [20]–[22]. Design of DAB DC-DC converter involves determining the turns ratio of the transformer and the series inductance [19], [23], [24]. Based on the worst-case stresses on the components, the design of magnetic components and selection of switches and capacitors can then be carried out.

In [23], the transformer turns ratio is chosen to obtain voltage conversion ratio of unity at maximum value of unregulated voltage while applying SPS strategy for power transfer. The inductance value is chosen to provide good controllability. This method is simple and widely used but it does not attempt to minimize rms inductor current or losses. In [24], a numerical design approach is adopted for selection of optimal transformer turns ratio and inductance value for minimization of rms inductor current averaged over several operating voltages at fixed power. Same method is used to minimize peak inductor current or total power loss which provide separate design parameter values. SPS strategy is considered for the analysis. It is well known in DAB literature [3], [8] that SPS results in large rms currents and loss of ZVS for wide variation of voltage and power. In [19], a numerical approach similar to [24] is taken but TPS with ZVS is considered and average efficiency is used as an objective function. Search is carried over a range of operating points resulting due to variations in unregulated port voltage and power.

Total loss or efficiency as an objective function is complex and requires knowledge of device and magnetics related parameters which are usually not known before the basic design is completed. In numerical search technique [19], [24], the search space is divided into discrete points and objective function is evaluated at each point to identify the optimum. This process is computation extensive, requires programming effort and does not provide much insight. Applying equal weightage to each operating point may not be practical.

This paper presents a novel analytical design procedure for a DAB DC-DC converter. The design specifications are the regulated port voltage, range of unregulated voltage, operating power range and switching frequency. Optimal TPS strategy is considered for the analysis which results in minimum rms current while ensuring soft switching. For accurate results, the minimization problem is formulated considering time domain analysis. Though it may seem obvious, it is established that maximum rms current with optimal TPS strategy flows at maximum power. This conclusion is independent of the choice of design parameters and the variation of voltage at the unregulated port. Minimization of the maximum rms current experienced by the converter over the operating range leads to optimal sizing of devices, filter capacitors and magnetics. A constrained optimization problem to minimize worst case inductor rms current is formulated and then solved analytically. The first order necessary conditions are applied on objective function to obtain algebraic equations for optimal variables. Since a closed form expression does not exist for one of the equations, a numerical root finding technique is used to find the optimal value. A polynomial curve-fit is then

provided for selection of the inductance value which reduces the computation effort. The solution thus obtained provides optimal values of the design variables (transformer turns ratio and inductance value). The proposed solution results in the maximum rms current (at maximum power) to remain close to its minimum value despite variations of voltage at the uncontrolled port. The optimal TPS strategy can be applied to the optimal design to obtain minimum rms currents and soft switching over the entire operating range of the converter. The key steps in selecting the power devices, filter capacitors and design of magnetics is also presented.

The rest of the paper is organized as follows. Section II describes the design problem and modelling of the converter for various zones of operation. An optimization problem is formulated for rms current minimization. A systematic procedure is discussed for the choice of design parameters. Section III demonstrates the experimental results with the proposed design strategy. Section IV concludes the paper.

## II. ANALYSIS & OPTIMAL DESIGN

Consider the dual active bridge DC-DC converter transferring power  $P$  between DC voltage sources  $V_1$  and  $V_2$  and switching at frequency  $f_s$  shown in Fig.1. The two H-bridge converters convert the DC voltages  $V_1$  and  $V_2$  to duty modulated square waveforms  $v_{ab}$  and  $v_{cd}$  respectively. These waveforms are then applied to a transformer connected in series with an inductor. The switches of the H-bridge converters are considered ideal and the effect of transformer magnetising inductance is neglected in the analysis. The inductor  $L$  in Fig.1 is the transformer leakage inductance along-with the external inductance. The converter can thus be equivalently replaced by two voltage sources and an inductor  $L$  as shown in Fig.2a. The power transfer between DC ports is carried out by introducing a phase shift between  $v_{ab}$  and  $v_{cd}$ .

A DAB converter can be modulated with three degrees of freedom (DOF). The primary and secondary voltage waveforms can be duty modulated. The pulse widths are decided by  $d_1 T_s/2$  and  $d_2 T_s/2$  for primary and secondary voltages

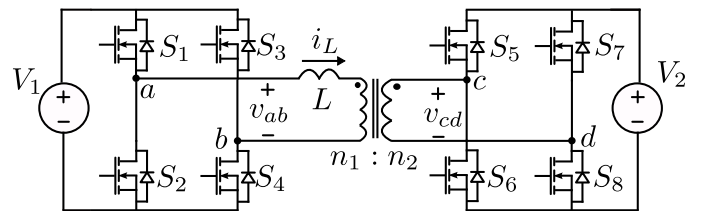


Fig. 1: A Dual active bridge DC-DC converter

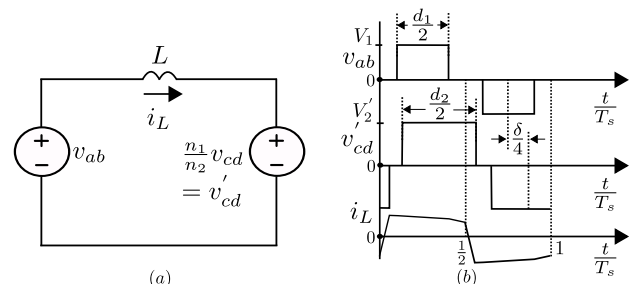


Fig. 2: (a) Equivalent Circuit of DAB, (b) Typical  $v_{ab}$ ,  $v_{cd}$  and  $i_L$  waveforms with 3-DOF control

respectively as shown in Fig.2b. The time-shift  $\delta T_s/4$  is provided for power transfer where  $T_s = 1/f_s$ . It can be seen from Fig.2b that the duty cycles  $d_1, d_2 \in [0, 1]$ . The phase shift ranges between  $-\frac{T_s}{4}$  and  $\frac{T_s}{4}$  which corresponds to  $\delta \in [-1, 1]$ .  $\delta > 0$  results in power transfer from  $V_1$  to  $V_2$ .

### A. Problem Description

Consider a DAB converter with the following specifications:

Port 1 Voltage:  $V_1$ , Switching Frequency:  $f_s$

Port 2 Voltage:  $V_{2min} \leq V_2 \leq V_{2max}$

Power Rating:  $P_{min} \leq P \leq P_{max}$

The problem above represents a scenario where one of the DC voltages ( $V_1$ ) is tightly regulated despite variations of  $V_2$ . The converter load also may vary between two known limits. Converter design involves determination of transformer turns ratio,  $n$  and value of series inductance  $L$ . After the design, the operation problem involves finding the modulation strategy ( $d_1, d_2$  and  $\delta$ ) for a given  $P$  and  $V_2$ . The specifications of inductor, transformer, switches and capacitor can then be determined based on worst-case operating conditions. The converter design should be carried out such that the maximum value of inductor rms current,  $I_{rms}$  is minimized over the entire operating range (considering variations in  $P$  and  $V_2$ ) of the converter. Moreover, zero voltage switching (ZVS) should be ensured for the entire operating region of the converter. Fulfilling these design objectives results in improved size and efficiency of the converter. The subsequent section discusses the converter model in steady state which is used for solving the optimization problem.

### B. Converter Modelling

The voltage conversion ratio is defined below where  $n_1$  and  $n_2$  are the number of turns in the transformer windings.

$$m = \frac{n_1 V_2}{n_2 V_1} = \frac{n V_2}{V_1} \quad (1)$$

For a given  $n$  and the variation of  $V_2$  described above,  $m$  varies between  $m_{min} := nV_{2min}/V_1$  and  $m_{max} := nV_{2max}/V_1$ . With the defined conversion ratio, the voltage levels in  $v_{cd}$  are  $\pm mV_1$  and zero. Note that the voltage levels in  $v_{ab}$  are  $\pm V_1$  and zero. The inductor current can be described by,

$$L \frac{di_L}{dt} = v_{ab} - nv_{cd} \quad (2)$$

Since the primary and secondary pulse widths are proportional to  $T_s$ , the inductor current magnitude is proportional to  $(\frac{V_1 T_s}{L})$  or  $(\frac{V_1}{2\pi f_s L})$ . Scaling the time axis with  $\theta = 2\pi f_s t$ , the inductor current at any time instant can be written as a product of  $\frac{V_1}{2\pi f_s L}$  and a proportionality factor  $i(m, d_1, d_2, \delta, \theta)$ . The actual rms current  $I_{rms}$  can then be written as,

$$I_{rms} = \frac{V_1}{2\pi f_s L} \sqrt{\frac{1}{2\pi} \int_0^{2\pi} i^2 d\theta} = \frac{V_1}{2\pi f_s L} i_{rms}(m, d_1, d_2, \delta) \quad (3)$$

Instantaneous power is the product of  $v_{ab}$  and the inductor current and hence will be proportional to  $\frac{V_1^2}{2\pi f_s L}$  with a

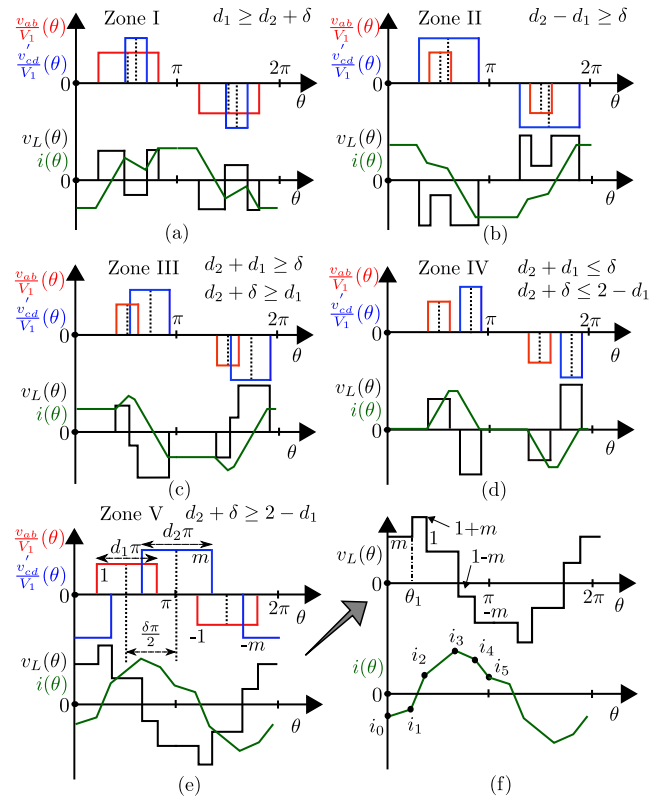


Fig. 3: DAB operating zones for  $d_1, d_2, \delta \in [0, 1]$

proportionality factor that is a function of  $m, d_1, d_2$  and  $\delta$ . The average power over a switching cycle can be written as,

$$P = \frac{V_1^2}{2\pi f_s L} \times p(m, d_1, d_2, \delta) \quad (4)$$

The values of  $i_{rms}$ ,  $p$  and the ZVS constraints are determined for various  $m, d_1, d_2$  and  $\delta$  in the subsequent sections.

1) *Converter operating zones*: The range of values that  $d_1, d_2$  and  $\delta$  can assume is between zero and one. So, each feasible point  $(d_1, d_2, \delta)$  belongs to a unit cube. This unit cube can be divided in five different operating zones where the expressions for  $p$  and  $i_{rms}$  are different because the inductor voltage has different pattern [3]. The different constraints in terms of operating variables  $[d_1, d_2, \delta]$  for each zone is depicted in Fig.3(a-e). Considering the transformation  $\theta = 2\pi f_s t$  to (2) described before, the dynamics in  $i$  can be described by the following equation,

$$\frac{di}{d\theta} = v_L(\theta) \quad (5)$$

where  $v_L(\theta) := (v_{ab} - v'_{cd})/V_1$  is the scaled inductor voltage. For operation of the converter in zone V, the values of  $v_L$  and  $i(\theta)$  at different time instants are indicated in Fig.3f. Considering the value of  $i$  at  $\theta = 0$  as  $i_0$ , the value of  $i_1$  can be determined from (5)

$$i_1 = i_0 + m\theta_1 \quad (6)$$

The values  $i_2-i_5$  can be similarly determined using (5). The inductor voltage  $v_L$  has half wave symmetry. Thus,  $i$  at steady state will be free from DC offsets and will have half wave

TABLE I: ZVS Constraints for different Operating Zones

Zone I	$(d_1 - d_2m) > 0$	$(\delta - d_2 + d_2m) > 0$	$(d_2 + \delta - d_2m) < 0$	
Zone II	$(d_1 - d_2m) < 0$	$(d_1m - d_1 + m\delta) < 0$	$(d_1 - d_1m + m\delta) > 0$	
Zone III	$(d_1 - d_2m) > 0$	$(d_2m - d_2 + \delta) > 0$	$(d_1 - d_1m + m\delta) > 0$	$(d_1 - d_2m) < 0$
Zone IV	$(d_1 - d_2m) > 0$	$(d_1 + d_2m) > 0$	$(d_1 - d_2m) < 0$	
Zone V	$(d_1 - 2m + m\delta + md_1) > 0$	$(d_2 + \delta + md_2 - 2) > 0$	$(\delta - d_2 + d_2m) > 0$	$(d_1 - d_1m + m\delta) > 0$

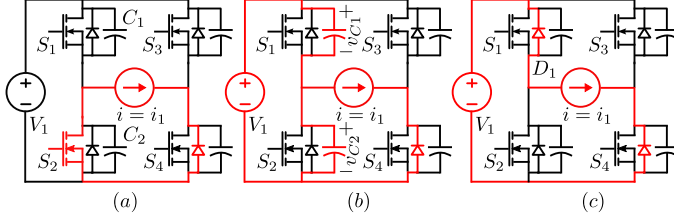


Fig. 4: Capacitor assisted soft switching

symmetry. This implies  $i_0 = -i_5$ . The values  $i_0 - i_5$  can now be determined as functions of  $m$ ,  $d_1$ ,  $d_2$  and  $\delta$ .

$$\begin{aligned}
 i_0 &= \frac{\pi}{2} (m - d_1 - m\delta) \\
 i_1 &= \frac{\pi}{2} (2m - md_1 - d_1 - m\delta) \\
 i_2 &= \frac{\pi}{2} (\delta + d_2 + md_2 - 2) \\
 i_3 &= \frac{\pi}{2} (\delta - d_2 + md_2) \\
 i_4 &= \frac{\pi}{2} (d_1 - md_1 + m\delta) \\
 i_5 &= \frac{-\pi}{2} (m - d_1 - m\delta)
 \end{aligned} \tag{7}$$

The scaled inductor current waveform  $i$  is determined for zone V. Similar analysis can be carried out for zone I-IV.

2) *Conditions for soft switching*: Consider that the converter is operating in zone V and undergoing the switching transition at  $\theta = \theta_1$  as shown in Fig.3f. At this instant, switch  $S_2$  is turning off and switch  $S_1$  is turned on after dead-time. This situation is depicted in Fig.4. Assume that the current  $i_1$  at  $\theta_1$  is less than zero. This implies that switch  $S_2$  was conducting prior to its turn-off and thus  $v_{C2} = 0$  (Fig.4a). On removing gate pulse for  $S_2$ , the inductor current quickly shifts to the capacitors  $C_2$  and  $C_1$ , charging and discharging them respectively (Fig.4b). The channel current quickly reduces before voltage  $v_{C2}$  increases and hence it reduces turn-off loss of  $S_2$ . Once the voltage  $v_{C1}$  reduces to zero, the diode  $D_1$  starts to conduct (Fig.4c). Turning on the switch after this instant will lead to ZVS turn on of  $S_1$ . Thus  $i_1$  should be less than zero for soft switching which

means  $(d_1 - 2m + m\delta + md_1) > 0$ . Evaluation of the current polarity condition for the remaining switching transitions leads to three more inequality constraints in  $m$ ,  $d_1$ ,  $d_2$  and  $\delta$ . A similar analysis can be carried out for zones I-IV. The set of inequality constraints are summarised in Table I.

From Table I, it can be concluded that ZVS conditions can be simultaneously satisfied in zones I, II and V only. All the transitions are not zero voltage switched in zones III and IV. Inequalities which cannot be satisfied simultaneously in zone III and IV are highlighted in Table I. Using the rms current expression in (3) and the current values from (7), the expression for  $i_{rms}$  is obtained in (9). Integrating the  $v_{ab}i_L$  product over half line cycle, the power  $p_{zV} = \frac{1}{2\pi} [(i_1+i_2)(\theta_2-\theta_1) + (i_2+i_3)(\theta_3-\theta_2) + (i_3+i_4)(\theta_4-\theta_3)]$ . Using the current expressions from (7) and time instants from Fig.3f, the scaled power is obtained in (8). The values of  $p$  and  $i_{rms}$  can be similarly evaluated for zones I and II. The expressions are indicated in (8) and (9).

### C. Optimal Modulation Strategy

In general, the inductor rms current is a function of  $n$ ,  $L$ ,  $V_1$ ,  $V_2$ ,  $P$ ,  $d_1$ ,  $d_2$  and  $\delta$ . In the design problem,  $V_1$  and  $f_s$  are fixed which from now onwards will be treated as known constants.  $V_2$  and  $P$  change over a range. Since  $n$  and  $V_2$  (both unknown at this point) appear to impact on  $I_{rms}$  and  $P$  as a product  $m = \left(\frac{nV_2}{V_1}\right)$ , their variation can be represented as  $m$ . The objective of design is to find  $n$  and  $L$  so that maximum rms current over a variation of  $V_2$  and  $P$  is minimized. As a first step, we need to determine  $I_{rms}$  as a function of  $m$ ,  $P$  and  $L$ . For one such given operating point ( $V_2$  and  $P$ ) and given  $n$  and  $L$  or in other words for a given  $P$ ,  $m$  and  $L$ , it is possible to find  $d_1$ ,  $d_2$  and  $\delta$  so that  $I_{rms}$  is minimized. This optimization problem where (3) is the objective function with (4) and ZVS conditions as the constraints is solved in [10]. The solution is known as optimal modulation strategy. Using (3) and (4) the problem can written as,

$$\min_{\substack{0 \leq d_1, d_2, \delta \leq 1, \text{ ZVS} \\ p = P \times (2\pi f_s L) / V_1^2 = \\ p|_m(d_1, d_2, \delta)}} i_{rms}|_m(d_1, d_2, \delta) \tag{10}$$

$$p_{zI} = 0.5m\pi\delta d_2 \quad p_{zII} = 0.5m\pi\delta d_1 \quad p_{zV} = 0.25m\pi (1 - (1 - d_1)^2 - (1 - d_2)^2 - (1 - \delta)^2) \tag{8}$$

$$\left. \begin{aligned}
 i_{rms,zI}^2 &= \frac{\pi^2}{12} (-2d_1^3 + 3d_1^2d_2m + 3d_1^2 - 6d_1d_2m - 2d_2^3m^2 + d_2^3m + 3d_2^2m^2 + 3d_2\delta^2m) \\
 i_{rms,zII}^2 &= \frac{\pi^2}{12} (d_1^3m - 2d_1^3 + 3d_1^2 + 3d_1d_2^2m - 6d_1d_2m + 3d_1\delta^2m - 2d_2^3m^2 + 3d_2^2m^2) \\
 i_{rms,zV}^2 &= \frac{\pi^2}{12} (-2d_1^3 - 3d_1^2\delta m + 3d_1^2m + 3d_1^2 + 6d_1\delta m - 6d_1m - 2d_2^3m^2 - 3d_2^2\delta m + \\
 &\quad 3d_2^2m^2 + 3d_2^2m + 6d_2\delta m - 6d_2m - \delta^3m + 3\delta^2m - 6\delta m + 4m)
 \end{aligned} \right\} \tag{9}$$

TABLE II: Boundary power levels [10]

	$p_{c1}$	$p_{c2}$
$m \leq 1$	$\frac{\pi m^2(1-m)}{2}$	$\frac{(1-m^2)\pi}{2m} \left( -1 + \frac{1}{\sqrt{1-m^2}} \right)$
$m > 1$	$\frac{\pi(m-1)}{2m}$	$\frac{m\pi}{2} (1-m^2 + m\sqrt{m^2-1})$

TABLE III: Optimum modulation parameters [10]

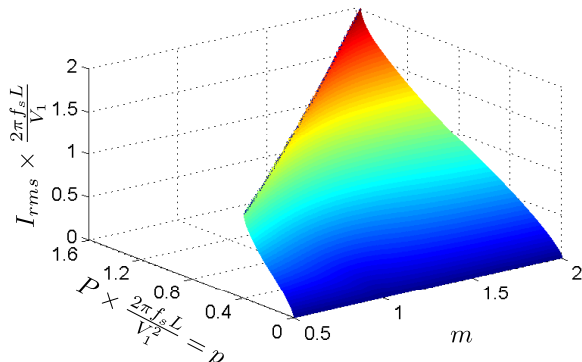
	$p \in [0, p_{c1})$	$p \in [p_{c1}, p_{c2})$
$m \leq 1$	$d_1 = \sqrt{\frac{2p}{(1-m)\pi}}$	$\pi d_1(1-\delta) = \pi m(2d_1 - d_1^2) - 2p$
	$d_1 = md_2$	$d_2 = 1$
	$\delta = (1-m)d_2$	$\delta = 1 - \sqrt{2d_1 - d_1^2 - \frac{4p}{m\pi}}$
$m > 1$	$d_1 = md_2$	$d_1 = 1$
	$d_2 = \sqrt{\frac{2p}{\pi m(m-1)}}$	$\pi d_2(1-\delta) = \frac{\pi}{m}(2d_2 - d_2^2) - \frac{2p}{m^2}$
	$\delta = (m-1)d_2$	$\delta = 1 - \sqrt{2d_2 - d_2^2 - \frac{4p}{m\pi}}$

Note that  $p|_m(d_1, d_2, \delta)$  implies  $p$  is a function of all four variables but  $m$  is treated as a constant. The solution depends on both  $m$  and  $p$ . For any given  $m$ ,  $p$  must be smaller than  $\frac{m\pi}{4}$  for solution of (10) to exist. Solution of the problem leads to three regions of operation [10]. For operating powers  $p$  upto  $p_{c1}$  (indicated in Table II, next page), the converter operates in zone I (zone II) for  $m > 1$  ( $m < 1$ ) with the modulation parameters listed in Table III. For  $p \in [p_{c1}, p_{c2}]$ , the modulation parameters are obtained by solving simultaneous equations in  $d_1$  and  $\delta$  for  $m \leq 1$  and in  $d_2$  and  $\delta$  for  $m > 1$ . These equations are indicated in second column of Table III. Beyond power levels of  $p_{c2}$ , the converter operates with the conventional phase shift strategy ( $d_1 = 1, d_2 = 1$ ). The value of  $\delta$  is given by  $\delta = 1 - \sqrt{1 - \frac{4p}{m\pi}}$ .

The optimal value of  $i_{rms}$  for various  $m \in [0.5, 2]$  and  $p \in [0, m\pi/4]$  is shown in Fig.5. It can be seen that for any fixed  $m$  (which means fixed  $nV_2$ ) and any arbitrary choice of  $L$  (provided  $p_{max} \leq m\pi/4$  is ensured), the value of  $i_{rms}$  (hence  $I_{rms}$ ) monotonically increases as  $p$  (or  $P$ ) is increased. Thus  $I_{rms}$  is maximum when  $P = P_{max}$ . It is now established that once  $m$  and  $L$  are fixed, the maximum value of rms current always occurs at  $P_{max}$ .

#### D. Design Problem Formulation

At this point we restate the design problem: (a)  $V_1$  and  $f_s$  are known and fixed quantities, (b)  $n$  and  $V_2$  appears as a product in (3) and (4) which is represented by  $m$ , (c)  $m$  and  $L$  needs to be determined so that rms inductor current  $I_{rms}$  is


 Fig. 5: Optimum value of  $i_{rms}$  for various  $m$  and  $p$ 

minimized for  $P = P_{max}$ . Substituting  $L$  (using  $P = P_{max}$  in (4)) in (3) we obtain (11)

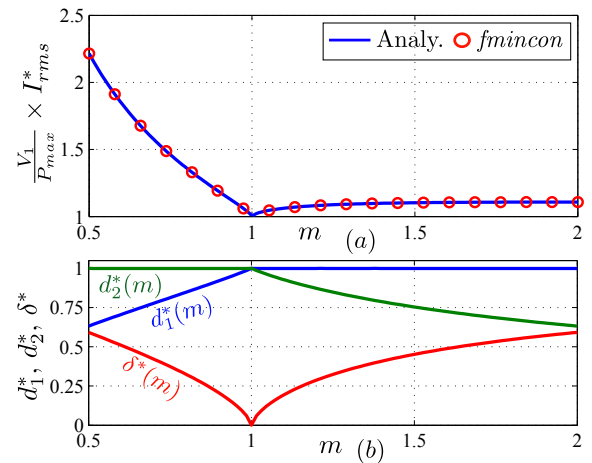
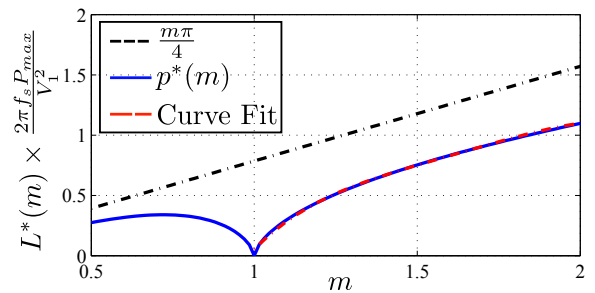
$$I_{rms} = \frac{i_{rms}(m, d_1, d_2, \delta)}{p(m, d_1, d_2, \delta)} \frac{P_{max}}{V_1} = \left( \frac{i_{rms}}{p} \right) \times \frac{P_{max}}{V_1} \quad (11)$$

As  $P_{max}/V_1$  is constant and known a priori from specifications, minimization of  $I_{rms}$  is equivalent to minimization of the ratio  $\left( \frac{i_{rms}}{p} \right)$ . Operation of the converter in zones I, II and V are considered since ZVS constraints can be only satisfied in these zones. For solving the multidimensional optimization problem  $m$  is fixed as a parameter and the optimal  $d_1^*$ ,  $d_2^*$  and  $\delta^*$  are determined which leads to minimum  $\left( \frac{i_{rms}}{p} \right)$  for that particular  $m$ . We obtain the following optimization problem with unknown variables  $m, d_1, d_2$  and  $\delta$ .

$$\min_{d_1, d_2, \delta \in [0,1]} \left( \frac{i_{rms}}{p} \right) \Big|_{m>0} (d_1, d_2, \delta) \quad (12)$$

#### E. Solution for a given $m$

Minimization of (12) is carried out by fixing  $m$  as a parameter and analytically solving the problem through KKT conditions. The ZVS conditions are met only in zone I, II and V which form mutually exclusive subsets of the unit cube. The optimization problem is solved in zones I, II and V separately and the minima among these three zones is identified. For the converter operating in zone V, the objective function to be minimized is  $\left( \frac{i_{rms,zV}}{p_{zV}} \right)$ . The expression for  $p_{zV}$  and  $i_{rms,zV}$  is given in (8) and (9) respectively. The


 Fig. 6: (a) Variation of optimum  $I_{rms}$  with  $m$  (b) Optimum operating point ( $d_1^*, d_2^*, \delta^*$ )

 Fig. 7: Optimum  $L^*$  (or  $p^*$ ) as a function of  $m$



$$(1 + m^2)^2 d_1^{*6} - 6m^2 (m^2 + 1) d_1^{*5} + 3m^2 (4m^2 + 1) d_1^{*4} - 2m^2 (5m^2 + 1) d_1^{*3} + 6m^4 d_1^{*2} - m^6 = 0 \quad (13a)$$

$$(1 + m^2)^2 d_2^{*7} - (2m^4 + 10m^2 + 8) d_2^{*6} + (15m^2 + 24) d_2^{*5} - (8m^2 + 34) d_2^{*4} + (4m^2 + 26) d_2^{*3} - 12d_2^{*2} - \frac{1}{m^2} d_2^* + \frac{2}{m^2} = 0 \quad (14a)$$

$$\delta^* = 1 - \frac{d_1^*}{m} + \sqrt{d_1^{*2} - 2d_1^* + \frac{d_1^{*2}}{m^2}} \quad (13b)$$

$$\delta^* = 1 - \frac{d_2^*}{m} + \sqrt{d_2^{*2} - 2d_2^* + m^2 d_2^{*2}} \quad (14b)$$

inequality constraints are given in the last row of Table I. Similar process is followed for zone I and II. The global optimum value of  $\left(\frac{i_{rms}}{p}\right)$  is found to be in zone V for all  $m > 0$ . For  $m \in [0, 1]$ ,  $d_2^* = 1$  and the value of  $d_1^*$  can be obtained by solution of equation (13a) in the range  $[0, 1]$ .  $\delta^*$  can be obtained from (13b). For  $m > 1$ ,  $d_1^* = 1$  and the value of  $d_2^*$  is obtained by determining the root of (14a) in the range  $[0, 1]$ .  $\delta^*$  can be obtained from (14b). The optimum value of the ratio  $\left(\frac{i_{rms}}{p}\right)^* = I_{rms}^* \times \frac{V_1}{P_{max}}$  is obtained for any given  $m$  by evaluating the ratio  $(i_{rms}/p)$  at  $d_1^*(m)$ ,  $d_2^*(m)$  and  $\delta^*(m)$ . This value is shown in Fig.6a (blue) for  $m \in [0.5, 2]$ . For validating the analytical solution, the optimization problem in (12) is solved numerically through *fmincon* package of MATLAB. The optimal rms current has close agreement with the analytical result (Fig.6a). The optimum modulation parameters are shown in Fig.6b. The values of  $d_1^*$ ,  $d_2^*$  and  $\delta^*$  for a given  $m$  can be substituted in the zone V power expression, (8) to obtain the value of  $p^*(m) = p(m, d_1^*, d_2^*, \delta^*) = \frac{2\pi f_s P_{max} L^*(m)}{V_1^2}$ . This process is repeated for other  $m$  and the result obtained is shown in Fig.7 (blue curve). Some important observations can be made from the solution.

- The global optimum of the problem occurs at  $m = 1$ . At this point  $d_1^* = 1$ ,  $d_2^* = 1$  and  $\delta^* = 0$ . This means  $p^* = 0$  (or  $L^* = 0$ ) and  $i_{rms}^* = 0$ . However, their ratio converges to unity. Operation at the global optimum point is thus not possible.
- As  $m$  is increased beyond 1, the value of  $I_{rms}^* \times \frac{V_1}{P_{max}}$  slowly increases from its global optimum of 1 and then stays almost constant at 1.1.
- For  $m < 1$ , the rms current increases rapidly as  $m$  reduces from unity. This value crosses 1.1 at  $m = 0.95$ . Thus, for achieving rms current less than or equal to 1.1 for an  $m < 1$ ,  $m$  must be greater than 0.95.

Fig.7 shows plot of  $p^*(m)$  and the maximum power  $\left(\frac{m\pi}{4}\right)$  which can be transferred for a given  $m$ . Close to  $m = 1$ ,  $p^*(m) \ll \frac{m\pi}{4}$  which implies poor controllability. For example at  $m = 0.95$ ,  $p^*(m) = 0.175$  is just 23% of the maximum power. This value reduces to zero as  $m = 1$  point is approached. So, it is not suggested to design  $L^*$  for  $m < 1$ .

### F. Fixing $m$ and finalizing design

Note that  $V_1$  and  $f_s$  are fixed and known a priori. For a given choice of  $m^*$ , the optimal value of inductance  $L^*$  is obtained by evaluation of  $p^*$  at  $m = m^*$ . For  $P = P_{max}$ ,  $L = L^*$  and  $m$ , the optimal modulation strategy as given in Section II-C can be used to obtain minimum rms current with soft switching. The optimal parameters can then be substituted in (9) to obtain the rms current. Now if we vary the chosen  $L^*$  which is same as changing  $m^*$  and repeat the process,

we obtain a set of curves with  $I_{rms}$  as a function of  $m$  with  $m^*$  as a parameter (cf. Fig.8). Note that for a given plot with particular  $m^*$ , the rms current will be minimum when  $m = m^*$ . This minimum current in Fig.8 (black dotted points) for a given  $m^*$  is same as the optimal rms current  $I_{rms}^*(m^*)$  in Fig.6a when  $m = m^*$ .

From the plots in Fig.8, it is possible to see that rms current rises faster with change in  $m$  for  $m < m^*$  when compared with  $m > m^*$ . Thus, the range of  $m$  in which we should operate must always be greater than  $m^*$  which implies  $m^* = m_{min}$ . For any given  $m^*$ , the rms current rises for  $m > m^*$ . From Fig.8, it can be observed that the rate of this current increase reduces with increasing  $m^*$ . This implies that a higher value of  $m^*$  should be chosen during design. With given converter specifications, the value of  $\gamma := \frac{m_{max}}{m_{min}} = \frac{V_{2max}}{V_{2min}}$  is known a priori. The ratio of rms currents at  $m_{max} = \gamma m^*$  and  $m_{min}$ , i.e.  $\frac{I_{rms}(m_{max} = \gamma m^*)}{I_{rms}(m^* = m_{min})}$ , for variation of  $m^*$  is indicated in Fig.9 (for different  $\gamma$ ). For a given value of  $\gamma$ , and a permissible limit on the variation of rms current, this curve can be used to determine  $m^*$ . For example with  $\gamma = 1.3$ , if we want the variation of rms current with respect to its minimum value to be less than 10%, then minimum  $m^* = 1.3$ . A higher value of  $m^*$  ( $> 1.3$ ) is not desirable since it leads to increase of the value of the required  $L^*$  (cf. Fig.7). Once  $m_{min} = m^*$  is fixed, the turns ratio is evaluated,  $n = m^* V_1 / V_{2min}$ . From subsection II-E,  $L = L^*(m^*) = p^*(m^*) \times \frac{V_1^2}{2\pi f_s P_{max}}$ . For determining  $L^*$ ,  $p^*(m)$  should be known which is given in Fig.7. A polynomial function is fitted on Fig.7 to determine  $p^*(m)$  once  $m$  is fixed.

$$p^*(m) = -1.9m^4 + 12.6m^3 - 30.9m^2 + 34.3m - 14.07 \quad (15)$$

For operation of the converter at points different than  $(P_{max}, V_{2min})$ , the modulation strategy described in section II-C is used [10]. The design steps are indicated as a flowchart in Fig.10. For a designed  $n$  and  $L$ , the per unit power varies between  $p_{min}$  and  $p_{max}$  and  $m$  varies between  $m_{min}$  and  $m_{max}$ . Thus, any operating point lies in a rectangle on  $m - p$

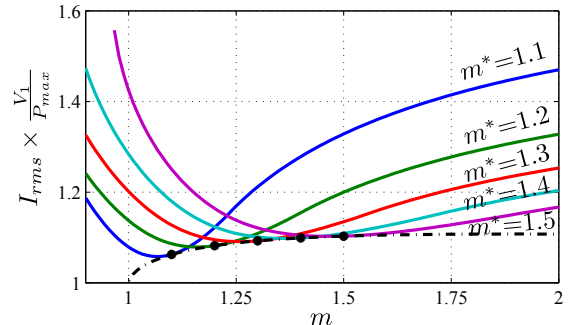


Fig. 8: Variation of rms current due to change in  $V_2$  (here  $m$ ) for a given  $L = L^*(m^*)$

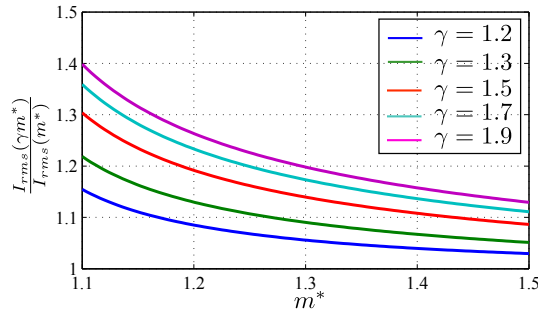


Fig. 9: Variation of  $\frac{I_{rms}(\gamma m^*)}{I_{rms}(m^*)}$  with  $m^*$  for various  $\gamma$

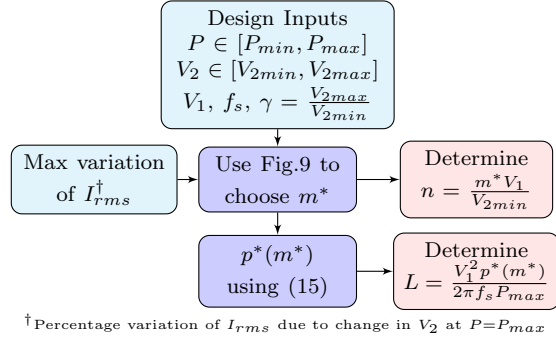


Fig. 10: Steps involved in converter design

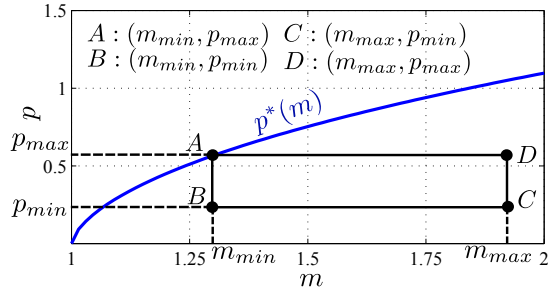


Fig. 11: Operating region of converter on  $m - p$  plane

plane bounded by the points A, B, C and D as shown in Fig.11. For  $P = P_{max}$  and  $\gamma = 1.3$  (say), the design strategy in Fig.10 gives  $m^* = 1.3$ . Thus,  $p_{max} = p^*(m = 1.3) = 0.56$ ,  $V_{2min}$  corresponds to  $m_{min} = 1.3$ . The point A on Fig.11 has coordinates  $(1.3, 0.56)$ ,  $m_{max} = 1.3 \frac{V_{2max}}{V_{2min}}$  and  $p_{min} = 0.56 \frac{P_{min}}{P_{max}}$ .

### G. Component Ratings

For a converter operating in the region shown in Fig.11, the maximum value of peak and rms currents need to be identified for switch selection. The rms current is maximum at operating point D ( $m_{max}, p_{max}$ ). The peak current is also maximum at D. The values of these currents can be determined using the design strategy in subsection II-F. The values of input and output ripple rms currents can be then be determined which decides the capacitor ratings (for a given primary and secondary voltage ripple  $\Delta V_1$  and  $\Delta V_2$  respectively). These values are indicated in Table IV. For designing the transformer, the area product needs to be determined. The core area is dependent on the volt-seconds applied to the magnetizing

TABLE IV: Device, Capacitor and Magnetics Rating

Switch	RMS	Peak	
Pri.	$0.84P_{max}/V_1$	$2.13P_{max}/V_1$	
Sec.	$0.84nP_{max}/V_1$	$2.13nP_{max}/V_1$	
Capacitor	Rip. RMS	Capacitance	
Pri.	$0.645P_{max}/V_1$	$0.1027P_{max}/(f_s V_1 \Delta V_1)$	
Sec.	$0.702nP_{max}/V_1$	$0.112nP_{max}/(f_s V_1 \Delta V_2)$	
Transformer	$A_c A_w$	$n$	$I_{rms}$
	$\frac{0.641P_{max}}{J f_s B_m k_w}$	$\frac{m^* V_1}{V_{2min}}$	$1.19 \frac{P_{max}}{V_1}$
Inductor	$A_c A_w$	$I_p$	$I_{rms}$
	$\frac{L I_p I_{rms}}{J B_m k_w}$	$2.13 \frac{P_{max}}{V_1}$	$1.19 \frac{P_{max}}{V_1}$

inductance which in this case is  $A_c = \frac{m V_1 d_2}{4 n_s n B_m f_s}$  where  $B_m$  is the peak flux density in core. The value of  $A_c$  is maximum when  $m$  and  $d_2$  are maximum. The worst-case value of rms current (which happens at point D) decides the window area since  $A_w = \frac{2 n_s n I_{rms}}{k_w J}$  where  $k_w$  and  $J$  are window factor and the current density respectively. The required area product is indicated in Table IV.

An external inductance may be required to be added in series with the transformer for obtaining the desired optimal  $L^*$ . In such a scenario, the required area product is given by  $A_c A_w = \frac{L I_p I_{rms}}{J B_m k_w}$ . The rms and peak values are shown in Table IV.

### III. EXPERIMENTAL RESULTS

To validate the converter design and operation methodology, a DC-DC converter was designed with the specifications provided in Table V using the method outlined in Section II-F. The value of  $m^*$  is chosen to be 1.3 which gives  $p^* = 0.56$ , resulting in  $n = 1.6$  and  $L = 73.13 \mu H$ . With these fixed values of  $n$ ,  $L$  and the modulation strategy described in Section II-C, the maximum transformer primary rms and peak currents (at  $P_{max}$ ,  $V_{2max}$ ) are 7.8 A and 14.0 A respectively. The secondary side rms and peak currents are 12.5 A and 22.4 A respectively. SiC MOSFETs (28 A current rating) are used for primary and secondary side switches. Isolated gate driver (ADuM4135) is used for generation of gating pulses. The primary and secondary capacitor ripple currents are calculated to be 4.29 A and 7.38 A respectively. Film capacitors of 2.5  $\mu F$  are used. The transformer area product is calculated to be  $9.26 cm^4$ . A planar transformer is ordered from Payton with turns ratio of 24 : 15 and area product of  $17.5 cm^4$ . The leakage inductance of the transformer is measured to be 20  $\mu H$  at 75 kHz. Accordingly, an external inductor of 53  $\mu H$  (area product:  $2.44 cm^4$ ) is designed using ferrite core (Part No: 0R45530EC). The experimental setup is shown in Fig.13. The values of  $d_1^* = 1$ ,  $d_2^* = 0.82$  and  $\delta^* = 0.35$  are obtained using the modulation strategy described in subsection II-C. Fig.12a shows the operation of the converter at point A ( $V_{2min} = 325$  V,  $P_{max} = 2.6$  kW). The converter operates in zone V (since  $d_1^* + d_2^* + \delta^* = 2.17 > 2$ ) for the set of modulation parameters which can be seen from Fig.12a. The experimental value of inductor RMS current is 7.14 A which is

TABLE V: Hardware Specifications

$V_1$	$V_{2min}$	$V_{2max}$	$P_{min}$	$P_{max}$	$f_s$
400 V	325 V	425 V	1 kW	2.6 kW	75 kHz

TABLE VI: Comparison at four operating points of converter

	$P$	$V_2$	$(d_1, d_2, \delta)$	$I_{rms}(T)$	$I_{rms}(S)$	$I_{rms}(E)$	Zone
A	2.6	325	(1.0, 0.82, 0.35)	7.18	7.23	7.14	V
B	1.0	325	(0.77, 0.59, 0.18)	3.28	3.23	3.23	I
C	1.0	425	(0.58, 0.34, 0.24)	3.79	3.74	3.69	I
D	2.6	425	(0.93, 0.55, 0.38)	7.78	7.65	7.42	I

close to the theoretically predicted RMS value as indicated in Table VI. The operating waveforms for four boundary points of the operating area with the modulation strategy in Section II-C are given in Fig.12b-d respectively. The converter operation is simulated in Simulink for the operating conditions in Fig.12. The modulation parameters along-with the theoretical (T), simulation (S) and experimental (E) rms currents for the four operating conditions are indicated in Table VI. A close agreement between theoretical, simulation and experimental values can be observed. It can be seen that for all these operating conditions, the power is less than  $\frac{nV_1V_2}{8f_sL}$  which is the maximum deliverable power. Thus, the converter is able to operate in the entire operating region of Fig.11.

### A. Soft Switching-Experimental Validation

Consider the converter operating in zone V at  $V_2 = V_{2min}$  and  $P = P_{max}$  (point A in Fig.11). Current  $i_1$  should be less than zero and the currents  $i_2, i_3$  and  $i_4$  should be greater than zero to ensure switch to diode transition (ZVS). For operation of the converter at point A, the currents  $i_1-i_4$  are indicated on Fig.12a. It can be seen that all the current polarities are maintained as desired which ensures soft switching. The

switching transition described in Section II-B2 (when  $i_L = i_1$ ) is shown in Fig.14 to demonstrate soft turn OFF of  $S_2$  and soft turn on of  $S_1$ . Switch  $S_2$  is conducting prior to its turn-off (at  $t_0$ ) since  $i_L = i_1 < 0$  (cf. Fig.12a). After  $t = t_0$ , the gate voltage  $v_{gs,S2}$  starts to reduce. The gate voltage reduces below threshold implying channel current is zero before  $v_{ds,S2}$  starts to increase at  $t = t_1$ . This results in ZVS turn-off of  $S_2$ . At  $t = t_2$ ,  $v_{ds,S1}$  reduces to zero and diode  $D_1$  starts conducting. The turn on of  $S_1$  at  $t = t_3$  happens at zero voltage indicating ZVS. Similar behaviour was observed for the remaining switching transitions of the converter.

### B. Efficiency and Loss breakup

The analytical and experimental converter efficiency is shown in Fig.15 for operation at minimum (along AB) and maximum (along CD)  $V_2$  (See Fig.11). A close agreement between the results can be observed. The peak efficiency of the converter is 97% for operation at  $V_2 = 325$  V. The efficiency of the converter is slightly reduced for operation of the converter at maximum  $V_2$  due to increased conduction losses.

Theoretical loss estimation is carried out for operation at the four boundary points in the operating area of the converter. A comparison of experimental loss and theoretical calculation is given in Fig.16a. Variation of on state resistance with current and dependence of core loss on temperature leads to slight mismatch between the values. A theoretical loss breakup for  $P_{max} = 2.6$  kW and  $V_{2min} = 325$  V (point A) is shown in Fig.16b. The primary and secondary switch rms currents are  $I_{rms}/\sqrt{2} = 5.08$  A and  $nI_{rms}/\sqrt{2} = 8.13$  A. With  $r_{ds,on} = 0.125$   $\Omega$  for primary and secondary MOSFETS,

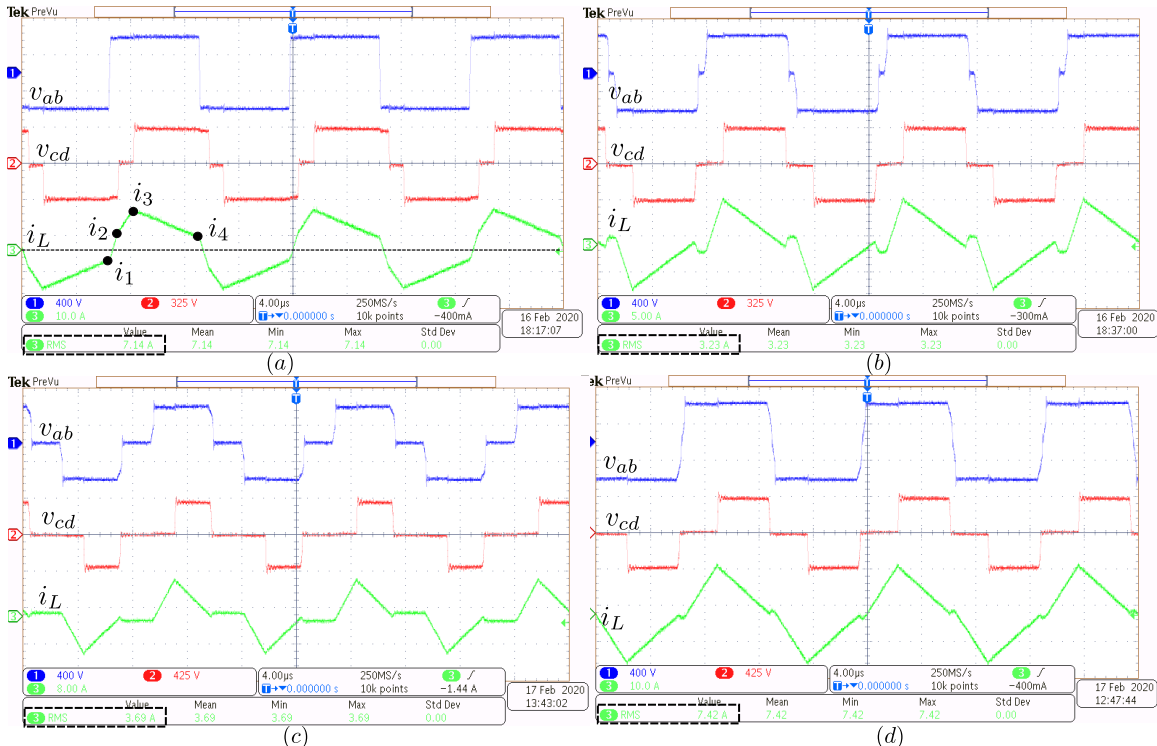


Fig. 12: Experimental results showing  $v_{ab}$ ,  $v_{cd}$ ,  $i_L$  and its RMS value for (a)  $P_{max} = 2.6$  kW,  $V_{2min} = 325$  V, (b)  $P_{min} = 1$  kW,  $V_{2min} = 325$  V, (c)  $P_{min} = 1$  kW,  $V_{2max} = 425$  V (d)  $P_{max} = 2.6$  kW,  $V_{2max} = 425$  V



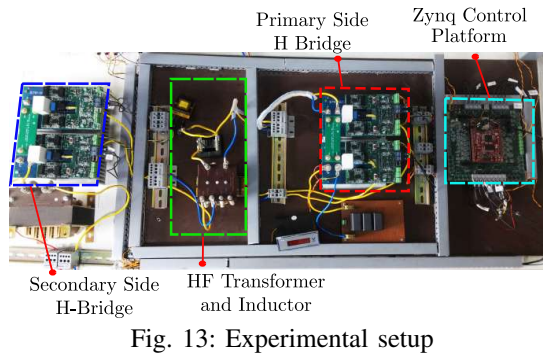


Fig. 13: Experimental setup

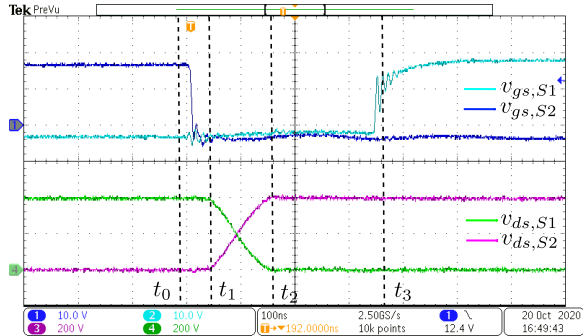
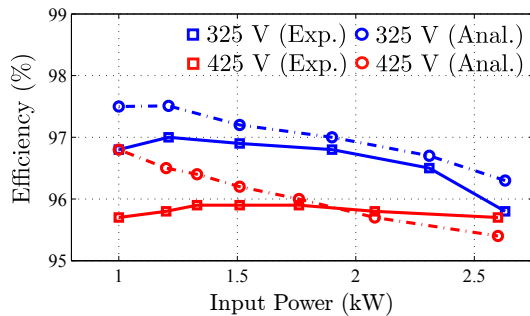
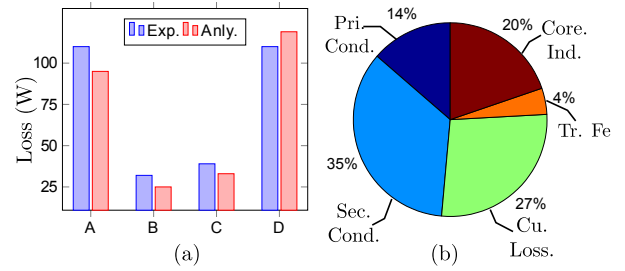

 Fig. 14: Experimental evidence of soft turn OFF of  $S_2$  and soft turn ON of  $S_1$  when  $i_L = i_1$  in Fig.12a


Fig. 15: Converter Efficiency

the primary and secondary conduction losses are 12.9 W and 33.04 W respectively. The transformer and inductor resistance is found to be  $r_c = 0.5 \Omega$  at 75 kHz. For rms current of 7.18 A (cf. Table VI), the conduction loss is 25.8 W. The core loss in transformer is evaluated through improved steinmetz equation. The core parameters  $\alpha = 1.098$ ,  $\beta = 2.196$ ,  $k_c = 0.025$  are obtained from the loss density curve given in the datasheet. The time averaged loss density is evaluated as  $\langle p_v \rangle = k_i |\Delta B|^{(\beta-\alpha)} \left| \frac{dB(t)}{dt} \right|^\alpha$  where  $\Delta B$  is peak-to-peak flux density. The empirical relation for  $k_i$  can be found in [25]. Evaluating  $\Delta B$  and  $\left| \frac{dB(t)}{dt} \right|$  from transformer applied volt-seconds,  $\langle p_v \rangle = 50.43 \text{ mW/cm}^3$ . Multiplying by the core volume the core loss in transformer is 4.13 W. This process is repeated for the inductor core ( $\alpha = 0.845$ ,  $\beta = 2.099$ ,  $k_c = 0.467$ ) and the core loss obtained is 18.66 W. The total loss at this operating condition is 94.8 W. It can be seen that major losses are the conduction losses in the bridges and copper losses in the transformer.


 Fig. 16: (a) Comparison of analytical and experimental losses for the operating points A, B, C, D in Fig.11 (b) Theoretical loss breakup for  $P_{max}=2.6 \text{ kW}$ ,  $V_{2min}=325 \text{ V}$ 

## IV. CONCLUSION

A design procedure for a dual active bridge based DC-DC converter with a given set of specifications (power range, uncontrolled port voltage range, controlled port voltage and switching frequency) is presented. The design is aimed at minimization of worst-case inductor rms current in the operating range of the converter. Modelling of the converter is carried out in time domain and optimal TPS strategy is considered for minimum rms current and soft switching in the entire operating range. It is identified that the maximum rms current with optimal TPS strategy always happens at maximum power. For the converter operating at maximum power and a given value of uncontrolled port voltage, an optimization problem is formulated for minimization of rms current with soft switching. Analytical solution of the optimization problem provides the optimal values of the design variables i.e. transformer turns ratio and the value of the series inductance. As the voltage of the uncontrolled port deviates from the value chosen for optimal design, the rms current deviates from its optimal value. Further analysis showed if the optimal design is done at the minimum value of the uncontrolled port voltage, the rms inductor current stays close to its optimal value, despite variation in the voltage. Closed-form expressions for optimal design variables obtained through curve-fitting are provided. A simple step by step procedure for obtaining the design parameter values from converter specifications is provided. Details of the selection of power devices, filter capacitors and design of transformer and inductor is also given. A 2.6 kW hardware prototype is designed based on the outlined procedure. Experimental results confirm the effectiveness of the design.

## APPENDIX

### A. Comparison with literature

A comparison of computational effort of the proposed method with [24] is provided in Table VII. The proposed method is simple to implement whereas the computational complexity is high in [24] for higher number of discrete points  $N$  in the range of optimization variables. A detailed performance comparison of the presented method with [23] is given. Same converter specifications (cf. Table V) are considered for both the methods. Following the design strategy in [23],  $n = 0.94$  and  $L = 78.4 \mu\text{H}$ . SPS modulation strategy is used. The worst case inductor rms,  $I_{rms}$  (same as input rms current,  $I_{rms,in}$ ) in [23] occurs for  $V_2 = V_{2min}$  and its

value is indicated in Table VIII. With the proposed design method, an improvement in the worst case rms current can be observed. A considerable reduction in the worst case peak current and the output rms current can be similarly observed. With the proposed design and modulation strategy in [10], the converter achieves soft switching in the entire operating range. With the strategy in [23], the converter is partially soft switched for low power and voltage.

For comparing the power density and component sizes, the area products of transformer, inductor and the capacitor ripple rms requirement are indicated in Table IX for both the methods. Area product and ripple rms currents are calculated for the method in [23] using the strategy in section II-G. Proposed method results in reduction of magnetic component and capacitor size. For comparing the efficiency, a loss comparison is provided in Table X for operation of the converter at  $P=2.6$  kW and  $V_2=325$  V. It can be seen that the proposed method results in reduction of conduction losses in both the bridges and copper losses in transformer and inductor. Thus the proposed method results in improvement of circuit performance in terms of efficiency, component size and worst case current stresses.

### B. Closed loop operation

The modulation technique in [10] is used for converter operation once design parameters are fixed according to section II-F. A closed loop voltage controller having structure as [10] is implemented in simulation and experiment for regulating the controlled port voltage to given value  $V_1^*$  during disturbances. The PI controller parameters are obtained as  $k_p=20$ ,  $k_i=25 \times 10^3$  following design process in [10]. Fig.17a shows the dynamic performance of the converter for step changes in load and  $V_2$ . The converter was initially operating with  $P=2$  kW,  $V_1=400$  V and  $V_2=325$  V. At  $t=1$  ms, the load of the converter is increased by 10% after which the closed loop action brings the delivered power to 2.4 kW and  $V_1$  to 400 V. At  $t=8$  ms,  $V_2$  is increased by 10%. The power settles to the same value after an initial short transient. For experimental verification, the response of the converter is shown in Fig.17b for a step change in  $V_1^*$  (CH4) from 360 V to 400 V. Following the step change at  $t=0$ , a first order dynamics can be observed in  $V_1$  after which it settles to 400 V (CH1). Since the load resistance is constant, the current accordingly increases from 4.5 A to 5 A (CH2). The measured power also increases to 2 kW.  $V_2$  is kept constant during this event (CH3).

TABLE VII: Computation comparison with [24]

Proposed strategy	Method in [24] with N discrete points
4 A, 16 M, 2 D, 0 S	$7N^3$ A, $22N^3$ M, $4N^3$ D, $2N^3$ S

A: addition, M: multiplication, D: division, S: square root

TABLE VIII: Worst Case performance comparison

	Factor	This paper	[23]
$I_{rms,in}, I_{rms}$ (Worst)	$\frac{P_{max}}{V_1}$	1.19	1.87
$I_{pk}$ (Worst)	$\frac{P_{max}}{V_1}$	2.13	2.54
$I_{rms,out}$ (Worst)	$\frac{P_{max}}{V_{2min}}$	1.64	1.84

TABLE IX: Comparison of component sizes

	Factor	This paper	[23]
Trans. $A_c A_w$	$\frac{P_{max}}{J f_s B_m k_w}$	0.641	0.935
Ind. $A_c A_w$	$\frac{P_{max}}{J f_s B_m k_w}$	0.229	0.459
Cap. Rip. RMS (Pri.)	$\frac{P_{max}}{V_1}$	0.645	1.581
Cap. Rip. RMS (Sec.)	$\frac{P_{max}}{V_{2min}}$	0.922	1.023

TABLE X: Loss comparison:  $P=2.6$  kW and  $V_2=325$  V

	Factor	This paper	[23]
Cond.-Pri.	$\left(\frac{P}{V_1}\right)^2 r_{on,p}$	2.387	6.996
Cond. - Sec.	$\left(\frac{P}{V_{2min}}\right)^2 r_{on,s}$	4.034	4.092
Copper Loss	$\left(\frac{P}{V_1}\right)^2 r_c$	1.194	3.498

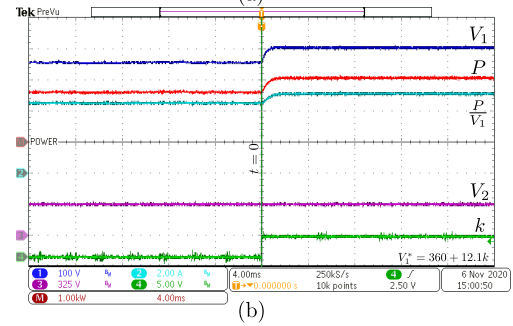
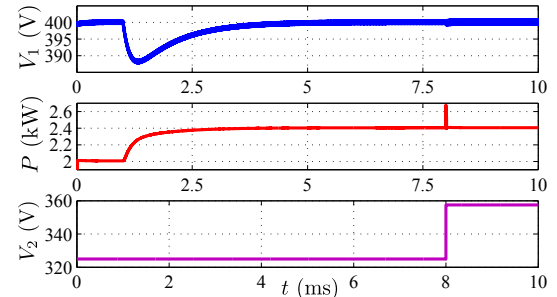


Fig. 17: (a) Simulation showing closed loop performance (b) Experimental result showing response to change in  $V_1^*$

### C. Discussion on EMC

The DAB circuit along-with LISN shown in Fig.18 is simulated to analyse the common mode noise. According to FCC regulation, the common-mode voltage ( $v_{cm} = 0.5(v_x + v_y)$ ) developed across  $50 \Omega$  resistance should be less than 1 mV in 150 kHz-30 MHz [27]. This regulation is violated without the EMI filter (cf. Fig.19a). An EMI filter is designed to attenuate the peak (150 mV) by 150 times (43.5 dB). Accordingly, LC filter (formed by  $L_{cm}$  and  $C_{cm}$ ) should have cut-off frequency of  $150 \times 10^{-43.5} = 12.24$  kHz. Fig.19b shows the common-

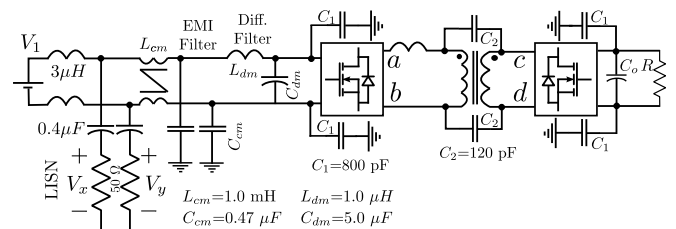


Fig. 18: Circuit to study EMC response ( $C_1$  &  $C_2$  from [26])

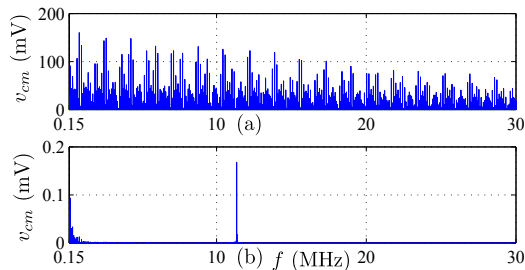


Fig. 19: Simulated EMC response without and with CM filter mode voltage spectrum with the EMI filter. It can be seen that the voltage is below 1 mV conforming to the regulation. Similar design can be carried out for load side.

## REFERENCES

- [1] R. De Doncker, D. Divan, and M. Kheraluwala, "A three-phase soft-switched high-power-density DC/DC converter for high-power applications," *IEEE Trans. Ind. Appl.*, vol. 27, no. 1, pp. 63–73, 1991.
- [2] M. Kheraluwala, R. Gascoigne, D. Divan, and E. Baumann, "Performance characterization of a high-power dual active bridge dc-to-dc converter," *IEEE Trans. Ind. Appl.*, vol. 28, no. 6, pp. 1294–1301, 1992.
- [3] A. K. Jain and R. Ayyanar, "PWM control of dual active bridge: Comprehensive analysis and experimental verification," *IEEE Trans. on Power Electron.*, vol. PP, no. 99, p. 1, 2010.
- [4] H. Bai and C. Mi, "Eliminate reactive power and increase system efficiency of isolated bidirectional dual-active-bridge DC/DC converters using novel dual-phase-shift control," *IEEE Trans. Power Electron.*, vol. 23, no. 6, pp. 2905–2914, Nov. 2008.
- [5] S. Wang, Z. Zheng, C. Li, K. Wang, and Y. Li, "Time domain analysis of reactive components and optimal modulation for isolated dual active bridge DC/DC converters," *IEEE Trans. on Power Electron.*, vol. 34, no. 8, pp. 7143–7146, Aug. 2019.
- [6] B. Zhao, Q. Song, W. Liu, G. Liu, and Y. Zhao, "Universal high-frequency-link characterization and practical fundamental-optimal strategy for dual-active-bridge DC-DC converter under PWM plus phase-shift control," *IEEE Trans. Power Electron.*, vol. 30, no. 12, pp. 6488–6494, Dec. 2015.
- [7] H. Shi, H. Wen, J. Chen, Y. Hu, L. Jiang, and G. Chen, "Minimum-reactive-power scheme of dual active bridge DC-DC converter with 3-level modulated phase-shift control," *IEEE Trans. Ind. Appl.*, vol. PP, no. 99, pp. 1–1, 2017.
- [8] F. Krismer and J. Kolar, "Closed form solution for minimum conduction loss modulation of DAB converters," *IEEE Trans. Power Electron.*, vol. 27, no. 1, pp. 174–188, 2012.
- [9] S. Chakraborty and S. Chattopadhyay, "Fully ZVS, minimum RMS current operation of the dual-active half-bridge converter using closed-loop three-degree-of-freedom control," *IEEE Trans. on Power Electron.*, vol. 33, no. 12, pp. 10188–10199, Dec. 2018.
- [10] A. Tong, L. Hang, G. li, X. jiang, and S. Gao, "Modeling and analysis of dual-active-bridge isolated bidirectional DC/DC converter to minimize rms current with whole operating range," *IEEE Trans. Power Electron.*, vol. PP, no. 99, pp. 1–1, 2017.
- [11] B. Zhao, Q. Song, W. Liu, and W. Sun, "Current stress optimized switching strategy of isolated bidirectional DC-DC converter with dual phase shift control," *IEEE Trans. on Ind. Electron.*, vol. 60, no. 10, pp. 4458–4467, Oct. 2013.
- [12] N. Hou, W. Song, and M. Wu, "Minimum current stress scheme of dual active bridge DC-DC converter with unified phase shift control," *IEEE Trans. on Power Electron.*, vol. 31, no. 12, pp. 8552–8561, Dec. 2016.
- [13] J. Huang, Y. Wang, Z. Li, and W. Lei, "Unified triple phase shift control to minimize current stress and achieve full soft switching of isolated bidirectional DC/DC converter," *IEEE Trans. on Ind. Electron.*, vol. 63, no. 7, pp. 4169–4179, Jul. 2016.
- [14] Q. Gu, L. Yuan, J. Nie, J. Sun, and Z. Zhao, "Current stress minimization of dual active bridge DC-DC converter within the whole operating range," *IEEE Journal of Emerging and Selected Topics in Power Electronics*, vol. 7, no. 1, pp. 129–142, Mar. 2019.
- [15] S. Shao, M. Jiang, W. Ye, Y. Li, J. Zhang, and K. Sheng, "Optimal phase shift control to minimize reactive power for a dual active bridge DC-DC converter," *IEEE Trans. on Power Electron.*, vol. 34, no. 10, pp. 10193–10205, Oct. 2019.
- [16] G. Oggier, G. O. Garcia, and A. R. Oliva, "Modulation strategy to operate the dual active bridge DC-DC converter under soft switching in the whole operating range," *IEEE Trans. on Power Electron.*, vol. 26, no. 4, pp. 1228–1236, Apr. 2011.
- [17] G. G. Oggier, G. O. Garcia, and A. R. Oliva, "Switching control strategy to minimize dual active bridge converter losses," *IEEE Trans. Power Electron.*, vol. 24, no. 7, pp. 1826–1838, Jul. 2009.
- [18] B. Zhao, Q. Song, and W. Liu, "Efficiency characterization and optimization of isolated bidirectional DC/DC converter based on dual phase shift control for dc distribution application," *IEEE Trans. on Power Electron.*, vol. 28, no. 4, pp. 1711–1727, Apr. 2013.
- [19] F. Krismer and J. W. Kolar, "Efficiency optimized high current dual active bridge converter for automotive applications," *IEEE Trans. Ind. Electron.*, vol. 59, no. 7, pp. 2745–2760, Jul. 2012.
- [20] U. Kundu, B. Pant, S. Sikder, A. Kumar, and P. Sensarma, "Frequency domain analysis and optimal design of isolated bidirectional series resonant converter," *IEEE Transactions on Industry Applications*, vol. 54, no. 1, pp. 356–366, Jan. 2018.
- [21] V. J. Thottuvelil, T. G. Wilson, and H. A. Owen, "Analysis and design of a push-pull current-fed converter," in *1981 IEEE Power Electronics Specialists Conference*, pp. 192–203, Jun. 1981.
- [22] J. Biela, U. Badstuebner, and J. W. Kolar, "Design of a 5kW, 1U, 10kW/dm<sup>3</sup> resonant DC-DC converter for telecom applications," *IEEE Transactions on Power Electronics*, vol. 24, no. 7, pp. 1701–1710, Jul. 2009.
- [23] C. Gammeter, F. Krismer, and J. W. Kolar, "Comprehensive conceptualization, design, and experimental verification of a weight-optimized all-sic 2 kV/700 V DAB for an airborne wind turbine," *IEEE Journal of Emerging and Selected Topics in Power Electron.*, vol. 4, no. 2, pp. 638–656, Jun. 2016.
- [24] V. M. Iyer, S. Gulur, and S. Bhattacharya, "Optimal design methodology for dual active bridge converter under wide voltage variation," in *2017 IEEE Transportation Electrification Conference and Expo (ITEC)*, pp. 413–420, Jun. 2017.
- [25] W. G. Hurley and W. H. Wölflé, *Transformers and inductors for power electronics: theory, design and applications*. John Wiley & Sons, 2013.
- [26] D. Bellan, "Symmetrical-component approach for circuit modeling of emi emissions in three-phase inverters," in *2019 IEEE PES Asia-Pacific Power and Energy Engineering Conference (APPEEC)*, pp. 1–5, 2019.
- [27] C. R. Paul, *Introduction to electromagnetic compatibility*, vol. 184. John Wiley & Sons, 2006.



**Dibakar Das** received the B.Tech degree from National Institute of Technology, Durgapur, India, in 2014 and M.S degree in electrical engineering from the Indian Institute of Science, Bangalore, India, in 2017. He is currently pursuing his Ph.D. in electrical engineering from Indian Institute of Science, Bangalore, India. His research interests include dual active bridge converters.



**Kaushik Basu** (S'07, M'13, SM'17) received the BE. degree from the Bengal Engineering and Science University, Shibpur, India, in 2003, the M.S. degree in electrical engineering from the Indian Institute of Science, Bangalore, India, in 2005, and the Ph.D. degree in electrical engineering from the University of Minnesota, Minneapolis, in 2012, respectively. He was a Design Engineer with Cold Watt India in 2006 and an Electronics and Control Engineer with Dynapower Corporation USA from 2013–15.

Currently he is an Associate Professor in the Department of Electrical Engineering in Indian Institute of Science. He has been an author and coauthor of several technical papers published in peer reviewed journals and conferences. His research interests include various aspects of the general area of Power Electronics. He is the founding chair of both IEEE PELS and IES Bangalore Chapter.